water

MDPI

Article

Temporal and Spatial Variations of Precipitation Change from Southeast to Northwest China during the Period 1961–2017

Zhu Li [1,2] and Honghu Liu [1,3,4,*]

1 State Key Lab Soil Erosion & Dryland Farming on the Loess Plateau, Institute of Soil and Water Conservation, Chinese Academy of Sciences and Ministry of Water Resources, Xinong Rd 26, Yangling 712100, China; lizhu19@mails.ucas.ac.cn
2 College of Modern Agricultural Sciences, University of Chinese Academy of Sciences, Beijing 100049, China
3 Changjiang River Scientific Research Institute, Changjiang Water Resource Commission, Wuhan 430010, China
4 Research Center on Mountain Torrent & Geologic Disaster Prevention of the Ministry of Water Resources, Wuhan 430010, China
* Correspondence: liuhh@mail.crsri.cn; Tel.: +86-278-292-6207

Received: 19 June 2020; Accepted: 4 September 2020; Published: 18 September 2020

Abstract: Global climate change is significant, and the spatiotemporal variations of precipitation associated with it are pronounced. Based on the daily precipitation data from 10 weather stations located from southeast to northwest across China from 1961–2017, the Mann–Kendall trend test was generally applied to analyze the spatiotemporal variations of precipitation. The factors influencing the precipitation changes were investigated. The results revealed that (1) the annual, summer, and winter rainfall amount (RA) exhibited increasing rates of 16.36, 12.31, and 2.49 mm/10 year, respectively. The change rates of annual rainfall days (RD) were 2.68 day/10 year in the northwest region and −1.88 day/10 year in the southeast. The annual and seasonal daily precipitation on rainy days (RP) exhibited an increasing trend. (2) All of the RA, RD, and RP values initially increased, then decreased, and then slightly increased from Southeast to Northwest China. These results proved that the RA increased with the increase of light rain in Northwest China and heavy rain in Southeast China. In addition, changes in the monsoon have altered the rate at which RA, RD, and RP vary with distance from the sea. These findings may help to provide suggestions for the rational spatial utilization of water resources in China.

Keywords: rainfall amount; rainfall days; daily precipitation; Mann Kendall trend test; Sen's slope; climate change

1. Introduction

Global warming may accelerate the hydrological cycle [1–4]. The accelerated hydrological cycle will affect the spatiotemporal patterns of precipitation, including the frequency of extreme precipitation events [5,6]. The frequent occurrence of extreme precipitation makes disasters, such as floods and droughts, more serious, which affects agricultural production and causes catastrophic destruction [7–10]. Therefore, there is an urgent need to study the spatiotemporal change of precipitation in order to mitigate the resulting natural disasters.

In recent years, many researchers have found that the intensity of precipitation events and the occurrence of extreme events have increased globally, although the spatiotemporal changes of precipitation in different regions of the world have not been the same [11–13]. (1) North America: Precipitation in Canada has exhibited an overall increasing trend with time [14–16]. Precipitation has

increased in the south, snow has increased in the north, and snow has decreased in the west [14,15]. Karl and Knight [17] (1998) reported that precipitation in the United States has increased since 1910, with the exceptions of Florida and California, with particularly heavy and extreme precipitation events [18,19]. (2) South America: Wang and Fu [20] (2002) explored the relationship between low-altitude cross-equatorial airflow and precipitation in South America, finding that the meridional wind was well-correlated with the zonal movement of precipitation in South America on the monthly time scale. Precipitation variation in the central region of the South American continent was mainly reflected in the south of Brazil. Precipitation in this region increased significantly from January to March, mainly due to the increase of rainy days [21]. (3) Europe: Zolina et al. [22] (2010) showed that the rainy season in most parts of Europe lengthened by approximately 15–20% from 1950 to 2008, and this prolonged wet period brought more heavy precipitation. According to Madsen et al. [23] (2014), some research has revealed that extreme precipitation in Europe is generally increasing, while there is no obvious trend of extreme flow at the large-scale regional or national level. Moreover, climate prediction indicates that extreme precipitation in Europe will generally increase in the future. (4) Africa: Kruger [24] (2006) reported that there has been no significant change in precipitation in most areas of South Africa, although there have been some significant changes in the precipitation characteristics of certain areas. For example, in the western region of South Africa, the degree of extreme drought has increased, corresponding to a significant decrease in the average rainfall in the southern summer [25]. (5) Asia: Precipitation in South Asia, Southeast Asia, and Central Asia has been mainly characterized by increased extreme precipitation [26–29], although the precipitation trend in most parts of Western Asia has been downward [30–32]. Sun and Ding [33] (2010) predicted that summer precipitation in East Asia will increase from 2010 to 2099. Zhai et al. [34] (2005) reported that the total precipitation in China from 1951 to 2000 exhibited almost no change trend, although there were obvious regional and seasonal trends: the precipitation in Northwest China increased significantly [35,36], southwest monsoon rainfall decreased overall [37], and the precipitation in South China was enhanced [38]. Zhang et al. [39] (2017) proved that the occurrence of extreme precipitation also increased in South China due to extension of the western North Pacific subtropical high westward, pushing tropical cyclones southward. Most of these studies concluded that global precipitation has changed, which can be inferred to have been the result of climate change. It remains unclear, however, to what extent climate change has impacted the variation of precipitation with distance to the sea from southeast to northwest China.

The purpose of this study was to investigate the temporal and spatial variations of precipitation from southeast to northwest China under global climate change and its possible influencing factors. This research included (1) the annual and seasonal changes of precipitation, (2) the changes of precipitation with distance from the sea, and (3) possible factors affecting spatiotemporal variation of precipitation. The results of this study provide a valuable support for the rational utilization and development of China's water resources.

2. Materials and Methods

2.1. Weather Stations and Data Collection

The daily precipitation and average daily temperatures data of ten meteorological stations from January 1961 to February 2018 were downloaded from the National Meteorological Center of the China Meteorological Administration (https://cmdp.ncc-cma.net/cn). There were some missing values in the daily precipitation dataset, although the total missing data was <0.1%. The discontinuous missing data were replaced by the average rainfall of adjacent days, and the continuous missing data were replaced by the long-term average of the same date, which would not affect the long-term trend change [4]. The meteorological stations selected in this study were observed and maintained in accordance with the ground meteorological observation standards of the China National Meteorological Administration. In addition, these data have undergone a strict quality control and inspection process, including

a consistency check, extreme value test, and so on. Following the quality control of the data, the actual data rate was generally more than 99%, and its accuracy rate was close to 100%. Based on the annual precipitation contours in China and their intersections of a straight line drawn from southeast to northwest [40], ten meteorological stations, namely, Fuzhou (FZ), Nanchang (NC), Wuhan (WH), Ankang (AK), Qindu (QD), Yuzhong (YZ), Xining (XN), Hongliuhe (HLH), Dabancheng (DBC), and Bole (BL) were selected (Figure 1). This ensured the relative integrity of daily precipitation data and the relative uniformity of spatial distribution of each station. Moreover, the annual precipitation of these ten meteorological stations represents the precipitation characteristics at various distances from the water vapor source: (1) FZ, NC, WH, and AK receive >800 mm, (2) QD receives 400–800 mm, (3) YZ and XN receive 200–400 mm, and (4) HLH, DBC, and BL receives <200 mm. Therefore, the differences in their precipitation should reflect the precipitation change from the southeast coast to the northwest inland areas of China. The basic information concerning these meteorological stations is listed in Table 1.

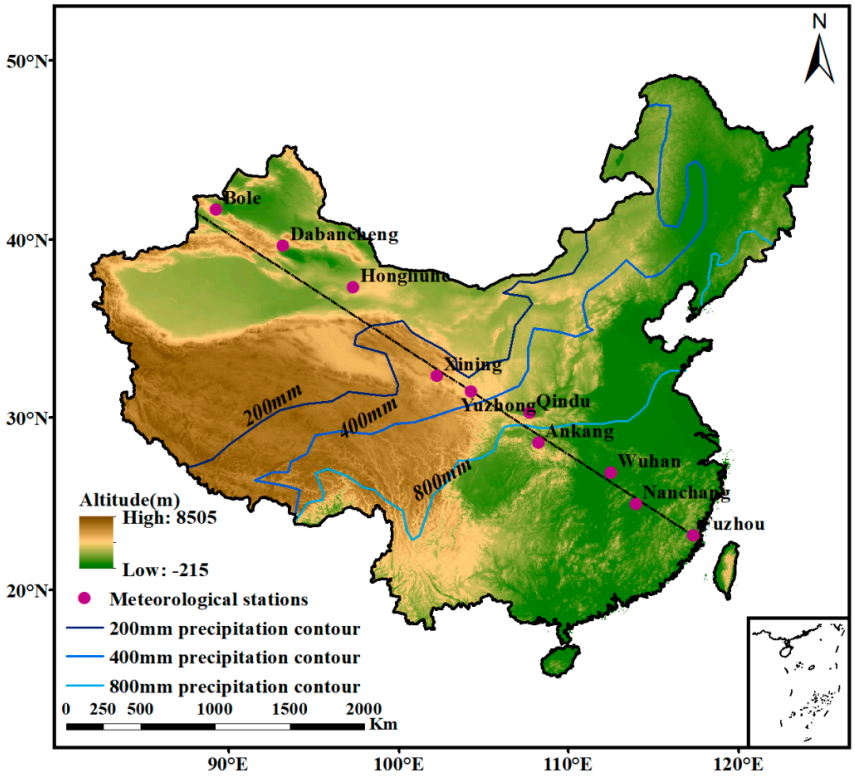

Figure 1. Digital elevation model (DEM) and distribution of the ten meteorological stations and precipitation contours.

Table 1. Basic information concerning the ten meteorological stations.

Station	Longitude (°E)	Latitude (°N)	Altitude (m)
Fuzhou (FZ)	119.17	26.05	84.00
Nanchang (NC)	115.55	28.36	46.90
Wuhan (WH)	114.03	30.36	23.60
Ankang(AK)	109.02	32.43	290.8
Qindu (QD)	108.43	34.24	472.80
Yuzhong (YZ)	104.09	35.52	1874.40
Xining (XN)	101.45	36.44	2295.20
Hongliuhe(HLH)	94.4	41.32	1573.8
Dabancheng (DBC)	88.19	43.21	1103.50
Bole(BL)	82.04	44.54	531.9

2.2. Data Preprocessing

2.2.1. Selection of Precipitation Indices

Three main indices and twelve sub-indices were determined based on the related studies (Table 2). These studies involved the statistics and descriptions of rainfall amount, rainfall days, and rainfall intensity, as well as the rainfall intensity of different grades during different time periods [28,41,42]. Although the abbreviations of these precipitation indices are different, their meanings are the same. In addition, these precipitation indicators only reflected annual or monthly statistics, due to a lack of seasonal statistics. In this study, a rainy day was defined as a daily rainfall amount ≥ 0.1 mm [41]. The total precipitation amount on rainy days divided by the corresponding number of rainfall days was defined as the daily precipitation on rainy days (RP), which was also a simple indicator for describing the rainfall intensity [28,42]. According to the classification system of the China Meteorological Administration, the daily precipitation was divided into four categories: light rain (LR, daily precipitation < 10 mm), moderate rain (MR, 10 mm ≤ daily precipitation < 25 mm), heavy rain (HR, 25 mm ≤ daily precipitation < 50 mm), and storm (SR, daily precipitation ≥ 50 mm). The rainfall amount (RA), rainfall days (RD), and daily precipitation on rainy days (RP) of the different rainfall grades were calculated in order to obtain the corresponding sub-indicators, as listed in Table 2. All of the indices were calculated for the corresponding seasonal and annual values.

Table 2. Precipitation indices considered in this study.

Index	Sub-Index	Unit
Rainfall amount (RA)	Light rainfall amount (LRA)	mm
	Moderate rainfall amount (MRA)	mm
	Heavy rainfall amount (HRA)	mm
	Storm amount (SRA)	mm
Rainfall days (RD)	Light rainfall days (LRD)	day
	Moderate rainfall days (MRD)	day
	Heavy rainfall days (HRD)	day
	Storm days (SRD)	day
Daily precipitation on rainy days (RP)	Daily precipitation on light rainfall days (LRP)	mm/day
	Daily precipitation on moderate rainfall days (MRP)	mm/day
	Daily precipitation on heavy rainfall days (HRP)	mm/day
	Daily precipitation on stormy days (SRP)	mm/day

2.2.2. Computation of Precipitation Indices

The annual and seasonal values of the 15 indices were calculated as follows: The first step was to determine the rainfall amounts (RA), including the annual and seasonal values, which were calculated from the daily values. We used standard climatological seasons to compute the seasonal values, that is, March–May for spring, June–August for summer, September–November for autumn, and December–February for winter. Different annual and seasonal RA grades were calculated, including light rainfall amount (LRA), moderate rainfall amount (MRA), heavy rainfall amount (HRA), and strong rainfall amount (SRA). The division of different precipitation grades adopted the precipitation division standard of the National Meteorological Center of the China Meteorological Administration; details are presented in the Note's section of Table 2. The multi-year RA averages for the periods 1961–2017, 1961–1990, and 1991–2017 were also calculated. The second step was to calculate the rainfall days (RD). The calculation method was the same as the approach used to calculate RA. The RD included the total RD, as well as RD for each of the four seasons every year; different annual and seasonal RD grades; and the multi-year RD averages for the periods 1961–2017, 1961–1990, and 1991–2017. The different RD levels included light rainfall days (LRD), moderate rainfall days (MRD), heavy rainfall days (HRD), and strong rainfall days (SRD). The third step was to calculate the daily precipitation on rainy days (RP), including the annual and seasonal values. We divided the RA by the RD of the corresponding period to obtain the RP for the same period. Different RP levels were also calculated, which included

daily precipitation on light rainfall days (LRP), daily precipitation on moderate rainfall days (MRP), daily precipitation on heavy rainfall days (HRP), and daily precipitation on stormy days (SRP).

2.3. Data Analysis

Five statistical analysis methods were selected to analyze the spatiotemporal variations of precipitation. These five data analysis methods comprise the following:

(1) Simple linear regression

The slopes of hydrometeorological variables over time and the associated long-term change trends can be measured by linear regression [42,43]. Simple linear regression was carried out for RA, RD, and RP with the change of distance from the sea, and the rates of decrease for the precipitation indices with distance from the sea were calculated.

(2) Mann–Kendall trend test

In this study, the Mann–Kendall (MK) trend test was used to detect the temporal trend changes of RA, RD, and RP. The MK trend test is a nonparametric method [44,45] and is recommended by the World Meteorological Organization for trend detection [46]. Since the autocorrelation in a time series will affect the results of the MK trend test, pre-whitening is used as a preprocessing method in order to eliminate this influence [47–49]. If there is a trend in the time series itself, the pre-whitening will weaken the test effect. When the sample size is large enough, however (generally > 50), there is no need for pre-whitening [50]. Since the sample size of each site in this study was >50, there was no need to pre-whiten.

For a given time series $X = x_1, x_2, \ldots, x_n$, MK test statistic S is calculated as:

$$S = \sum_{i=1}^{n-1} \sum_{j=i+1}^{n} \operatorname{sgn}\left(x_j - x_i\right) \tag{1}$$

The function sgn(x) is calculated as:

$$\operatorname{sgn}(x) = \begin{cases} 1, & x > 0 \\ 0, & x = 0 \\ -1, & x < 0 \end{cases}$$

The statistic S is approximately normally distributed, and the mean $E(S) = 0$, variance as:

$$\operatorname{Var}(S) = \frac{n(n-1)(2n+5) - \sum_{i=1}^{n} t_i(i)(i-1)(2i+5)}{18} \tag{2}$$

where t_i is the number of connections with sample i. The standardized test statistic Z is given by the following formula:

$$Z = \begin{cases} \frac{S-1}{\sqrt{\operatorname{Var}(s)}}, & S > 0 \\ 0, & S = 0 \\ \frac{S+1}{\sqrt{\operatorname{Var}(s)}}, & S < 0 \end{cases} \tag{3}$$

For the statistical value Z, when it is greater than 0, it is an increasing trend, and when it is less than 0, it is a decreasing trend.

(3) Sen's slope estimator

Sen's slope is an unbiased estimation of the monotonic trend of the original data, which can determine the true slope of the MK trend analysis [51,52]. In this study, it was used to measure the magnitude of the time variation trends of RA, RD, and RP. The calculation is as follows:

$$\beta = \text{Median}\left(\frac{x_i - x_j}{i - j}\right) \quad (4)$$
$$1 < j < i < n$$

When $\beta > 0$, it means an upward trend, and if $\beta < 0$, it means a downward trend. Otherwise, there is no change trend.

(4) Correlation analysis

Pearson correlation coefficient was used to detect the relationship between precipitation indices and temperature. Pearson correlation coefficient between precipitation index and temperature was calculated in OriginPro 9.0 software, and significance testing was performed by a double-tail test [53].

(5) Contrastive analysis and relative distance

The standard climate period is not unified worldwide. When studying climate change, researchers select different climate periods, with correspondingly different results [54]. Since the Intergovernmental Panel on Climate Change (IPCC) has reported many times that the standard climate period is 1961–1990, the standard climate period in this study was chosen to be 1961–1990. The comparative analysis of precipitation between the standard climate period and 1991–2017 was used to reflect the precipitation change under climate change.

When calculating the distance from the sea, this study used the relative distance. Using the "Measure" button in ArcGIS 10.2 software, we took the FZ station as the origin and measured the distance from the other 9 stations to FZ. These measurements represented the corresponding distances of the stations from the sea. Also taking Fuzhou as the starting point, a straight line was drawn from FZ to the northwest, in order to select other stations distributed near the straight line. The precipitation contours of 200, 400, and 800 mm each intersected this line. Similarly, ArcGIS 10.2 software was used to measure the distance between each intersection point and the FZ station, thereby yielding the distances of different precipitation contours from the sea.

3. Results

3.1. Temporal Change of Precipitation from Southeast to the Northwest China

3.1.1. Interannual Trend Changes of Annual Precipitation Indices

The interannual trends of RA, RD, and RP for the ten weather stations are presented in Figure 2. First, the annual RA of FZ, NC, WH, AK, XN, HLH, DBC, and BL all exhibited obvious increasing trends, while QD and YZ displayed decreasing trends. The average annual RA rising speed in the whole southeast to northwest line region was about 16.36 mm/10 year, while the slopes of FZ, NC and WH were all greater than 30 mm/10 year. Second, starting from YZ station, the annual RD in the southeast direction showed a downward trend and the average changing rate was about −2.68 days/10 year, while the annual RD in the northwest direction showed an upward trend and the average changing rate was about 1.88 days/10 year. The changing rates at WH, AK and QD reached −6.2, −2.73, and −3.33 day/10 year, respectively, and all exceeded the significance level of 95% confidence. Third, only the annual RP at YZ exhibited a slight downward trend, while the other nine stations all presented obvious upward trends. The growth rates at FZ, NC, WH, AK, QD, XN, HLH, DBC, and BL were represented by Sen's slope as 0.42, 0.39, 0.66, 0.28, 0.2, 0.07, 0.06, 0.11, and 0.09 mm/day/10 year, respectively. And the average annual RD rising speed in the whole southeast to northwest line region was about 0.23 mm/day/10 year. These results confirmed that the annual precipitation from southeast to northwest China changed from 1961 to 2017, although different precipitation indices had different change trends.

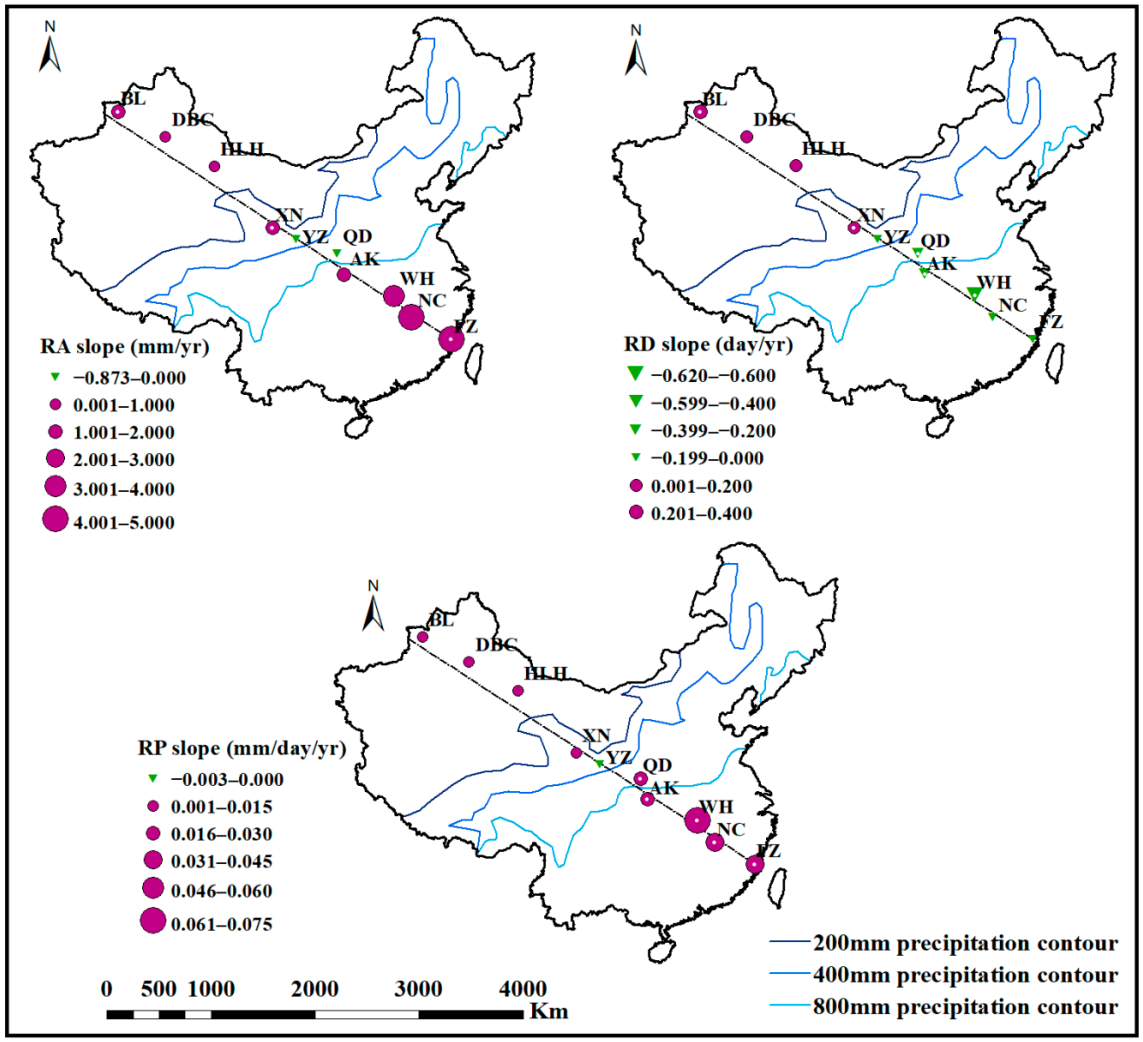

Figure 2. The Mann-Kendall trend test and Sen's slope were used to reflect the variation trends for the annual rainfall amount (RA), rainfall days (RD), and daily precipitation on rainy days (RP). Note: white spots mean precipitation change trend reached the significance level of 95% confidence according to the MK trend test.

3.1.2. Interannual Trend Changes of Seasonal Precipitation Indices

Figure 3 shows the interannual trend changes of selected spring precipitation indices. First, spring RA of YZ and in the northwest direction of YZ both showed an upward trend and the average Sen's slope of these stations reached 1.42 mm/10 year, while in the southeast direction of YZ both showed a downward trend and the average Sen's slope of these stations reached 4.77 mm/10 year. Second, spring RD of YZ and in the northwest direction of YZ both no obvious trend of change and all of these stations have a slope of 0 except for XN station, which presented an upward trend with a growth rate of 0.66 day/10 year. However, RD in the southeast direction of YZ showed a significant downward trend, and the average changing rates of these stations was −1.27 day/10 year. Third, the spring RP of all stations on the line from southeast to northwest showed an upward trend, except for AK and QD sites. And the average changing rate of spring RP of all stations reached 0.13 mm/day/10 year. Moreover, the RP of WH had a significant upward trend with a slope of 0.64 mm/day/10 year, which was caused by the significant decline in the number of precipitation days. Since there was no obvious change in the RA of WH, it can be inferred that the heavy rainfall of WH increased.

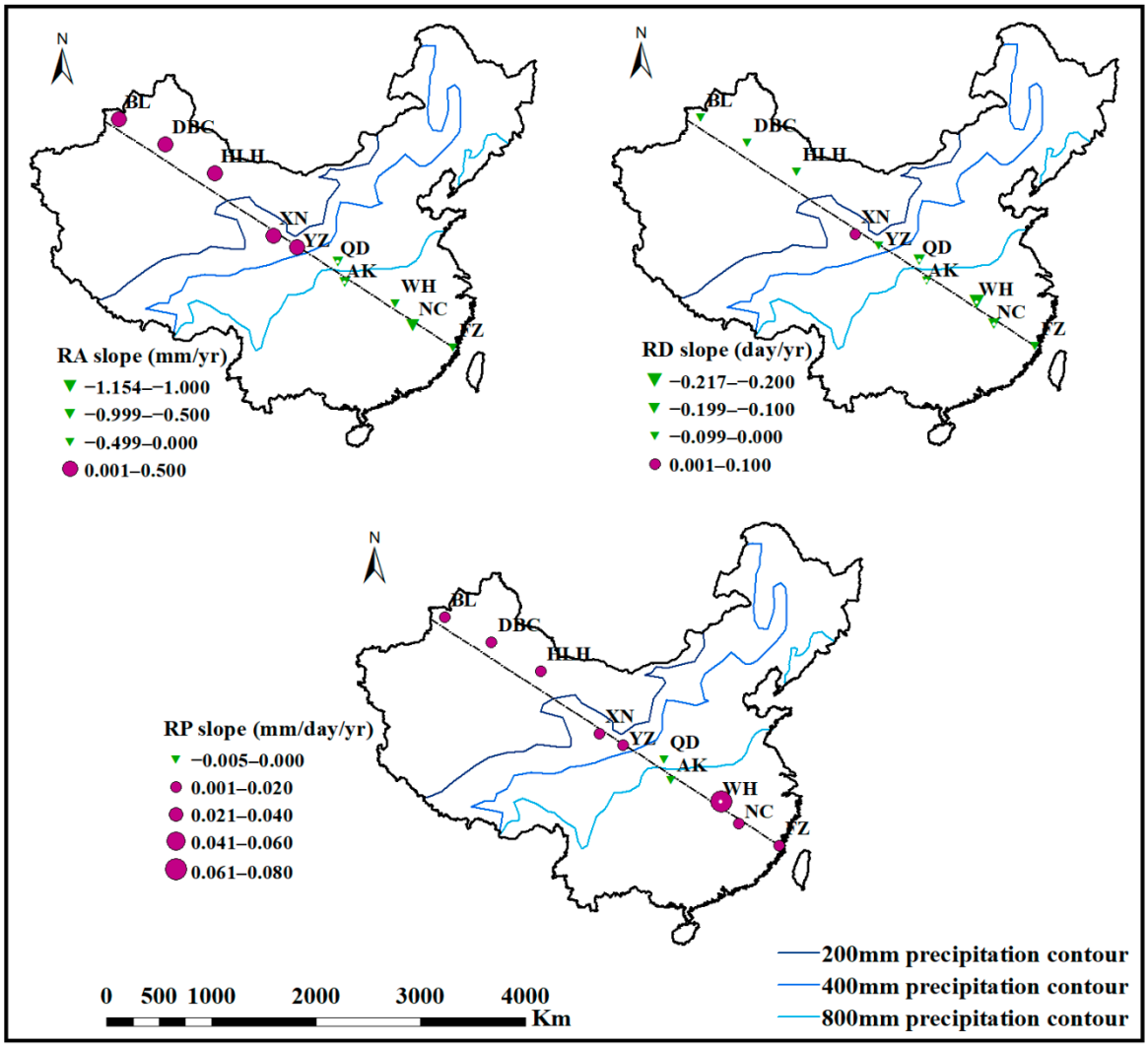

Figure 3. The Mann-Kendall trend test and Sen's slope were used to reflect the variation trends for the spring precipitation indices, including rainfall amount (RA), rainfall days (RD), and daily precipitation on rainy days (RP). Note: white spots mean precipitation change trend reached the significance level of 95% confidence for the MK trend test.

Figure 4 shows the interannual trend changes of selected summer precipitation indices. First, summer RA of all stations on the line from southeast to northwest showed an upward trend, except for YZ sites. And the average changing rate of summer RA of all stations reached 12.31 mm/10 year. Second, there was no change of summer RD at WH, AK, QD, and HLH, and changing rate of these stations was 0. The summer RD at YZ decreased significantly, with a changing rate of −0.83 day/10 year. However, FZ, NC, XN, DBC, and BL exhibited growth trends in RD, with ascent rates of 0.28, 1.18, 0.5, 0.51, and 0.51 day/10 year, respectively. Third, the summer RP did not change significantly at YZ, while the other stations all exhibited increasing trends. The growth rates of summer RP at XN, HLH, DBC, and BL were <0.15 mm/day/10 year. The growth rates of summer RP at FZ, NC, WH, AK, and QD were all >0.4 mm/day/10 year, with WH reached 0.96 mm/day/10 year. Further, the average changing rate of summer RP of all stations reached 0.35 mm/day/10 year.

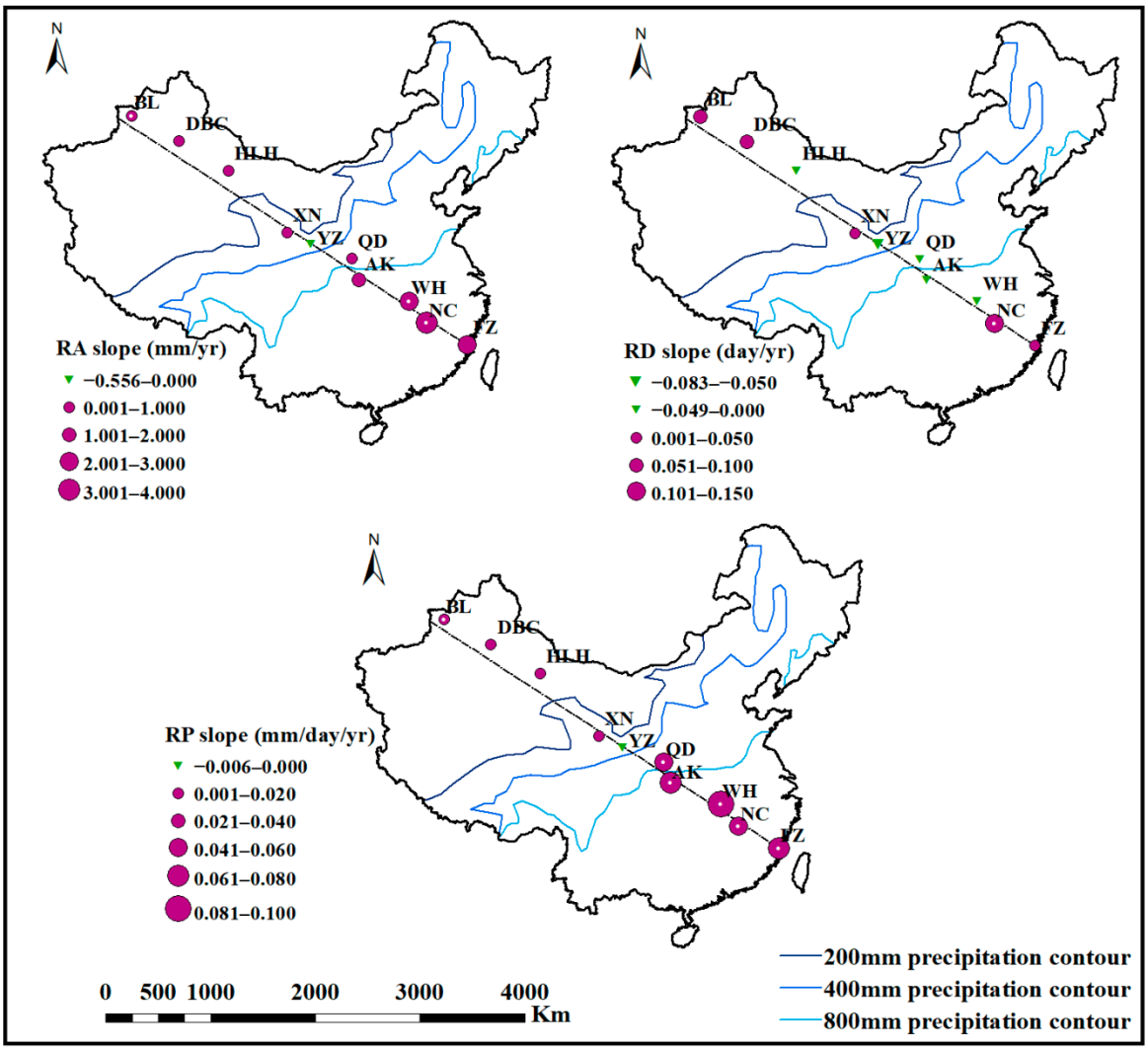

Figure 4. The Mann-Kendall trend test and Sen's slope were used to reflect the variation trends for the summer precipitation indices, including rainfall amount (RA), rainfall days (RD), and daily precipitation on rainy days (RP). Note: white spots mean precipitation change trend reached the significance level of 95% confidence for the MK trend test.

Figure 5 shows the interannual trend changes of selected autumn precipitation indices. First, the autumn RA changes of FZ, NC, XN HLH, and BL showed an increasing trend, and other stations showed a decreasing trend. Second, autumn RD in the northwest direction of YZ both showed a slight upward trend, and the average Sen's slope of these stations reached 0.24 day/10 year. However, autumn RD in the southeast direction of YZ showed a significant decreasing trend, and the average changing rate of these stations was up to −1.42 day/10 year. Third, the autumn RP of YZ showed a slight downward trend, while other stations all showed an upward trend. The average annual RP rising speed in the whole southeast to northwest line region was about 0.16 mm/day/10 year. According to the change trend of autumn RA and RD of YZ, the decline of RP was caused by the decreased of RA, so it can be inferred that the heavy precipitation in autumn decreased.

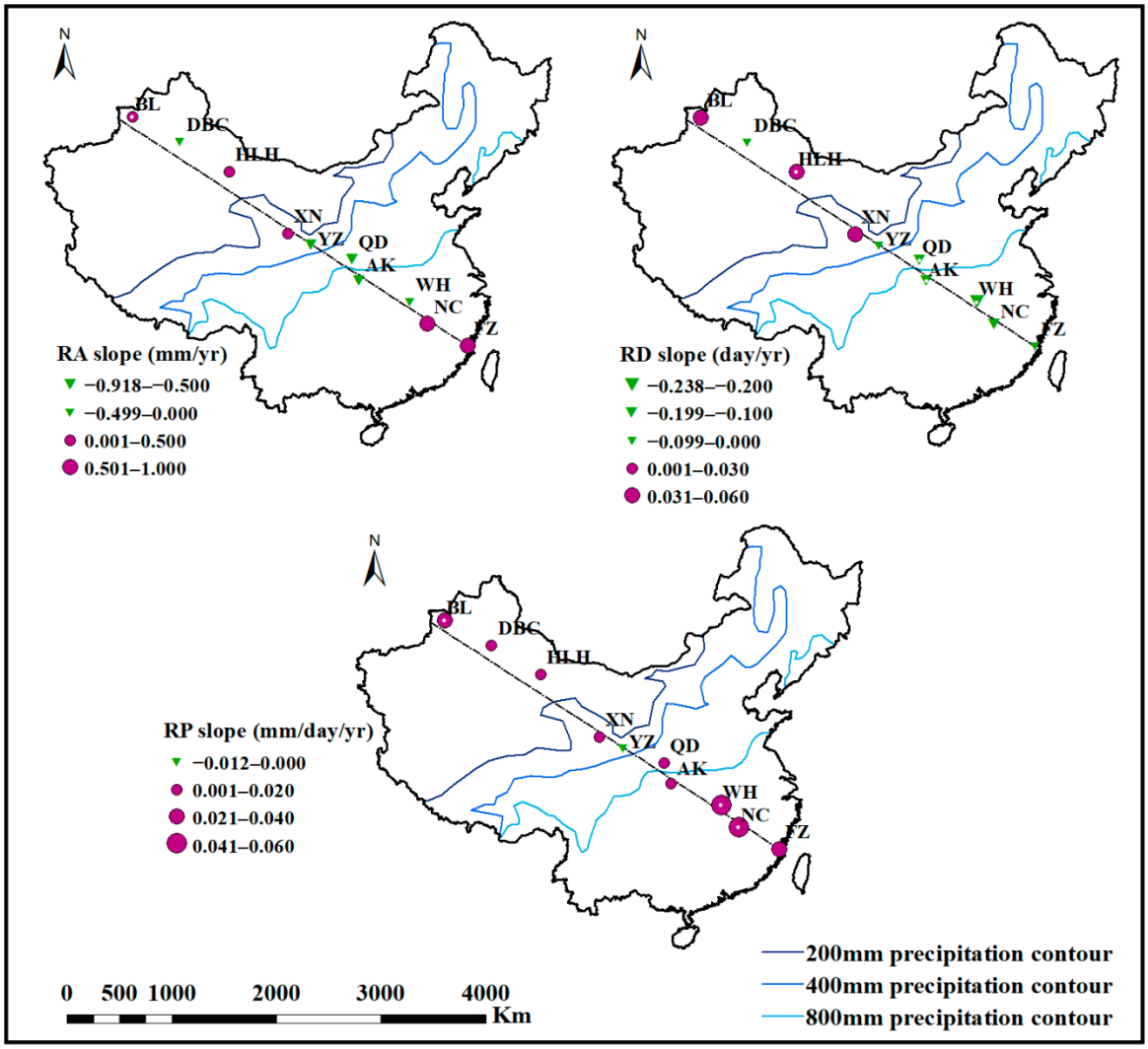

Figure 5. The Mann-Kendall trend test and Sen's slope were used to reflect the variation trends for the autumn precipitation indices, including rainfall amount (RA), rainfall days (RD), and daily precipitation on rainy days (RP). Note: white spots mean precipitation change trend reached the significance level of 95% confidence for the MK trend test.

Figure 6 shows the interannual trend changes of selected winter precipitation indices. First, the growth trends of winter RA at all of the ten stations were obvious, and the average growth rate of these stations was 2.49 mm/10 year. Second, the winter RD before the 800 mm precipitation contour all decreased, and the average changing rate of these four stations was −0.74 day/10 year. Winter RD of QD and in the northwest direction of QD both showed a significant upward trend, and the average ascent rate of these stations was up to 1.08 day/10 year. Third, the winter RP at all of the ten stations displayed obvious growth trends, and the average ascent rate of all these stations was 0.18 mm/day/10 year.

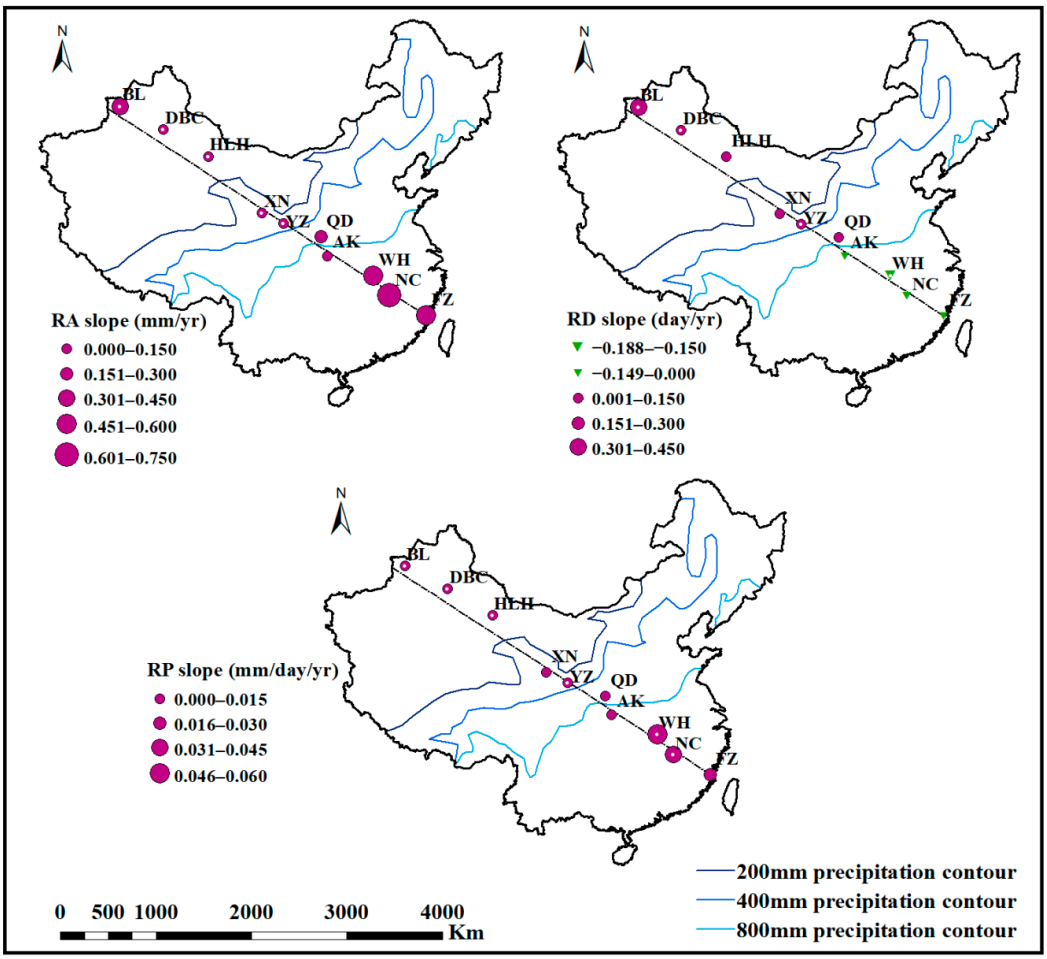

Figure 6. The Mann-Kendall trend test and Sen's slope were used to reflect the variation trends for the winter precipitation indices, including rainfall amount (RA), rainfall days (RD), and daily precipitation on rainy days (RP). Note: white spots mean precipitation change trend reached the significance level of 95% confidence for the MK trend test.

It can be concluded that (1) RA showed an upward trend in annual, summer and winter during the study period. Spring and autumn RA showed a slight upward trend in arid and semi-arid regions and a downward trend in humid and semi-humid regions; (2) annual, summer, autumn and winter RD were significantly increased in arid and semi-arid regions, and decreased in humid and semi-humid regions. RD dropped significantly in spring; and (3) annual and seasonal RP exhibited an upward trend. Therefore, the precipitation trend in annual was similar to that in summer and winter. It can be inferred from these results that the precipitation changes mainly occurred during the summer and winter because the monsoon changed in the summer and winter. In addition, RP responds to rainfall intensity, so it can be inferred that different levels of rainfall have changed during the study period.

3.2. Spatial Variation of Precipitation Indices from Southeast to the Northwest China

3.2.1. Spatial Variation of Precipitation Indices from 1961 to 2017

Figure 7 shows the changes of RA, RD, and RP with distance from the sea. Figure 7 can be analyzed from several perspectives. First, both RA and RP exhibited nearly the same change trends. In general, annual, spring, summer, autumn, winter RA and RP all decreased with the increase of the distance from the sea, but the decrease extent was different. Specifically speaking, in spring, summer and winter RA and RP first increased from FZ station to NC station, then gradually decreased to HLH station and then slightly increased to BL station. RA values of the first four weather stations

were basically the same in autumn, which gradually decreased from AK to HLH station and then increased slightly to BL station. In autumn, RP decreases slowly from FZ station to HLH station and then increases slightly to BL station. Secondly, on the whole, annual and seasonal RD first decreased greatly and then increased slightly with the increase of distance from the sea. But annual and summer RD appeared to rise in YZ and XN stations. And the first four stations of autumn RD rose slowly with the increase of the distance from the sea. On the whole, the precipitation indices decreased with the increase of distance from the sea. However, there were also local phenomena that rainfall increased with the increase of distance from the sea. It can be inferred from these results that the distribution of precipitation distance from the sea may be influenced not only directly by the monsoon, but also by factors such as topography.

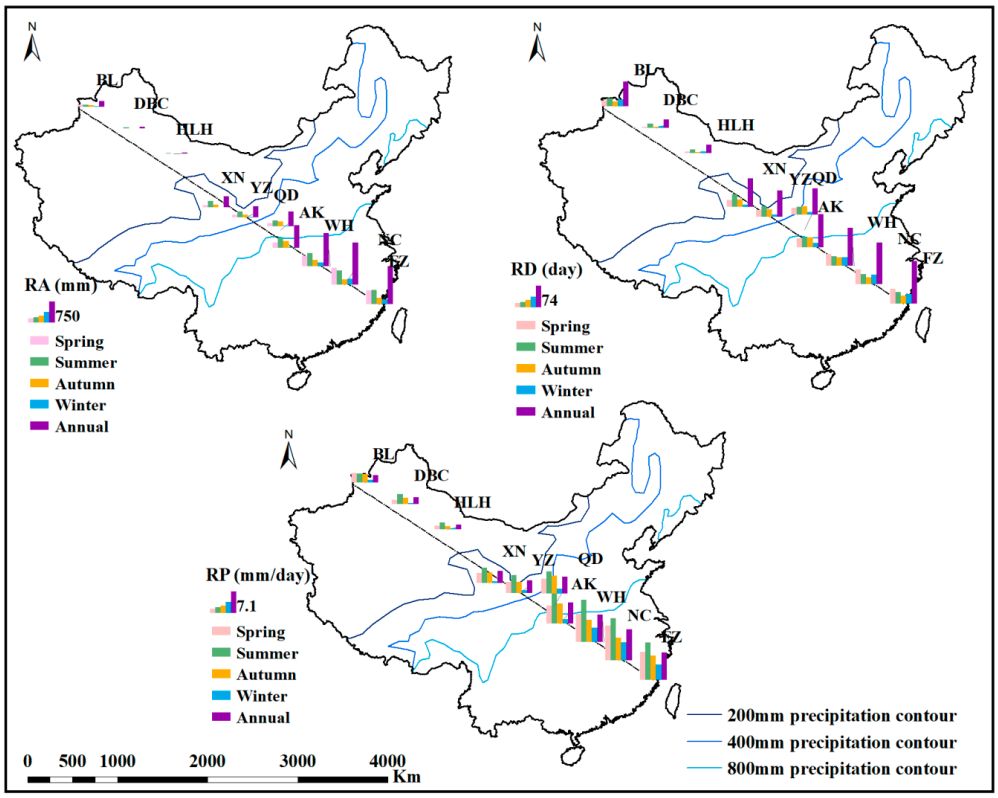

Figure 7. Spatial changes of precipitation indices with distance from the sea. Precipitation indices included rainfall amount (RA), rainfall days (RD), and daily precipitation on rainy days (RP).

3.2.2. Comparison of Precipitation Indices between 1961–1990 and 1991–2017

Figure 8 displays the annual and seasonal changes of RA, RD, and RP with distance from the sea between 1961–1990 and 1991–2017. The precipitation indices from 1991 to 2017 were compared with those of the standard climate period 1961–1990. Some conclusions can be drawn from Figure 8: (1) The annual RA changed very little, with the exception of NC, while the annual RD decreased significantly. Pronounced RD reductions appeared at FZ, NC, WH, AK, and QD. These decreases caused the annual RP at these 5 meteorological stations to increase. The annual RP at the DBC station also exhibited an obvious change (Figure 8a). (2) The spring RA and RP changed very little, while the spring RD before the 400 mm precipitation contour decreased significantly (Figure 8b). (3) The summer and winter precipitation indices were very similar to the annual indices (Figure 8c,e), although the magnitude of the increase or decrease was different. And the summer RA before the 800 mm precipitation contour increased significantly, while the winter RD after the 400 mm precipitation contour increased significantly. In addition, summer RD changed very little, although the summer RP increased a great deal (Figure 8c). (4) The autumn precipitation indices differed from the annual

indices, as well as those of the other seasons. The autumn RA before the 400 mm precipitation contour except FZ and NC stations decreased significantly, and the autumn RD before the 400 mm precipitation contour decreased even more (Figure 8d). Conversely, the autumn RP increased.

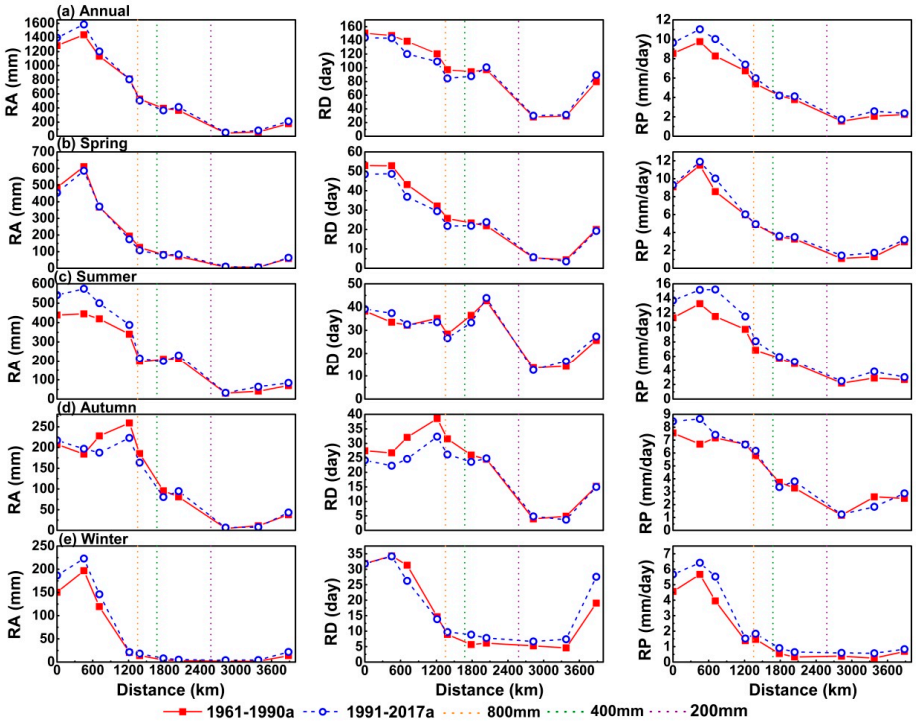

Figure 8. Changes of rainfall amount (RA), rainfall days (RD), and daily precipitation on rainy days (RP) with distance from the sea from 1961–1990 and 1991–2017, including the annual (**a**) and seasonal (including spring (**b**), summer (**c**), autumn (**d**) and winter (**e**)) changes. "800 mm" represents the 800-mm precipitation contour; "400 mm" represents the 400-mm precipitation contour; "200 mm" represents the 200-mm precipitation contour.

3.2.3. Spatial Variation of Precipitation Index Change Trends from 1961 to 2017

Figure 9 shows the change rates of the annual and seasonal RA, RD, and RP with increasing distance from the sea. First, the time trend slope of RA in year and summer was similar with the change of distance from the sea, and both decreased with the increase of distance from the sea. However, there was a slight upward trend from FZ to NC, and the decline in QD station was large, reaching the minimum value in YZ. Moreover, HLH, DBC and BL showed a slight upward trend. However, the RA slope in spring, autumn and winter fluctuated slightly with the increase of sea distance (Figure 9a). Second, the RD slope in summer and winter did not change significantly with the distance from the sea. The slope of RD in spring and autumn decreased first and then increased with the increase of sea distance. The annual RD slope increased as a whole with the increase of distance from the sea, but the minimum value appeared at WH (Figure 9b). Third, the slope of annual RP was similar to that of four seasons RP with the change of distance from the sea, which increased first, then decreased, and finally tended to be stable. But the minimum RP slope of annual and summer appeared in YZ, while spring appeared in QD and winter in AK. And the maximum RP slope of spring appeared in NC, while annual and other three seasons all appeared in WH (Figure 9c). It should be noted that the obvious negative RA slope occurred in humid and semi-humid regions for spring and autumn, while the RD slopes at FZ, NC, WH, AK, QD, and YZ were also negative except summer and winter RD. The negative RP slopes were at the AK and QD station in spring and the YZ station in annual, summer, and autumn. This may reflect the degree to which climate change has affected rainfall as a function of distance from the sea.

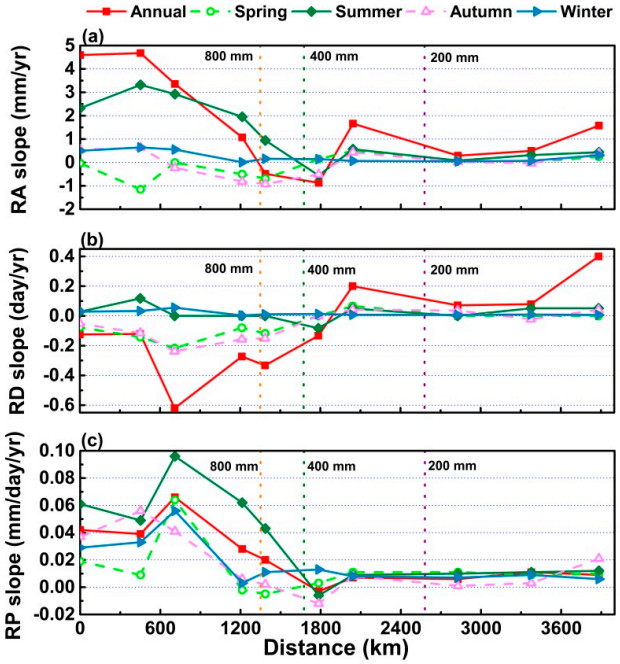

Figure 9. Spatial variation of Sen's slope of the MK trend test for selected precipitation indices, including (**a**) rainfall amount (RA), (**b**) rainfall days (RD), and (**c**) daily precipitation on rainy days (RP) with distance from the sea. "800 mm" represents the 800-mm precipitation contour; "400 mm" represents the 400-mm precipitation contour; "200 mm" represents the 200-mm precipitation contour.

In a word, the half of annual and seasonal RA and RP declined, and the trend changes were similar, which showed RP can better reflect the trend of RA. The most dramatic decrease and descent rate of RD, respectively, occurred at the WH and QD stations. In fact, the RP at the first three stations in summer, winter and annual exhibited obviously increasing trends. These results imply that the annual monsoon intensity strengthened, but the monsoon frequency in spring and autumn weakened. Their impacts were felt as far as 3500 km from the coast (DBC station) and 2000 km from the coast (XN station).

4. Discussion

4.1. Comparison of These Research Results with Those of Other Studies

In general, the summer, winter, and annual RA changes displayed increasing trends, although the annual RA decreased at the QD and YZ stations and summer RA also decreased at YZ. The spring RA did not change significantly, while the autumn RA decreased significantly. Zhai et al. [34] (2005) also found that the annual RA increased significantly in the western part of China, the Yangtze River Valley, and the southeast coastal region. The summer RA trend was very similar to the annual trend; the RA in eastern China generally decreased in autumn; and the winter RA in the northern part of eastern China decreased significantly, while increasing in the south. Many researchers have confirmed that the annual RA in Northwest China has exhibited an obviously increasing trend [35,36,55–57]. The fact that the RA has increased in winter and summer but decreased in spring and autumn has been recognized by most researchers [55,58,59]. There has been a significant increase in the RA of long-duration events in southern China [60]. The RA from southeast to northwest China has generally decreased with increasing distance from the sea. This change has been confirmed by many scientists [59,61,62]. The annual and seasonal RA decrease at different rates with distance from the sea. In recent years, these descent rates have also changed, with the annual, summer, and winter RA descent rates increasing significantly, while the descent rate has reversed in the spring and autumn (Table 3). In addition, we found that the RA increased from the FZ to NC stations, but decreased sharply at QD (Figure 7).

Meanwhile, the time trend slope of the winter RA increased with distance from the sea, while the annual, spring, summer, and autumn RA initially decreased, then increased with increasing distance from the sea.

Annual, summer, autumn and winter RD were significantly increased in arid and semi-arid regions, and decreased in humid and semi-humid regions; the RD in spring decreased significantly. Zhai et al. [34] (2005) also found that the RD has decreased in most parts of China, with Northwest China being an exception. The annual wet days (daily precipitation >1 mm) increased in Northwest China, with the northern part of Northwest China increasing significantly, while the eastern part decreased as far west as 100° E [63]. Feng and Zhao [59] (2015) reported that the RD in China exhibits a decreasing trend to the southeast. The RD in southeastern to northwestern China generally decreased with increasing distance from the sea. The annual and seasonal RD decreased at different rates with sea distance. In recent years, this descent rate has also changed, with the descent rates of the annual, spring, autumn, and winter RD decreasing, although there was faint change in summer (Table 3). In addition, the time trend RD slope did not change significantly in summer, although the annual, spring, autumn, and winter slopes initially decreased at the WH station (750 km from the coast), then increased, illustrating the variation of RD with distance from the sea. At the FZ and QD stations, however, the annual and seasonal RD changes were not consistent.

The seasonal and annual RP changes generally exhibited increasing trends, and the increasing trend of RP in winter was significant. Zhai et al. [34] (2005) also found that the RP has increased noticeably in China. The increase of RP was mainly concentrated in the lower reaches of the Yangtze River and the Pearl River Basin, while the northern part of northwestern China has also exhibited characteristics of increasing RP [63]. The RP of southeast to northwest China also decreased generally with increasing distance from the sea. The annual and seasonal RD decreased at same rate with sea distance. In recent years, the descent rates of annual and seasonal RP have both increased (Table 3). In addition, we found that the RP increased from the NC to WH stations, but decreased sharply at QD (Figure 7). The time trend RP slope was similar to that of RA, which had a peak value at the WH station and a minimum at the YZ station.

Table 3. Simple linear regression slope of rainfall amount (RA), rainfall days (RD), and daily precipitation on rainy days (RP) versus sea distance from 1961–1990 and 1991–2017.

Slope	Years	Annual	Spring	Summer	Autumn	Winter
RA (mm/km)	1961–1990	−0.3664	−0.1392	−0.1198	−0.0638	−0.0431
	1991–2017	−0.3884	−0.1313	−0.1469	−0.0605	−0.0502
	Comparison	−0.0220	0.0079	−0.0270	0.0033	−0.0071
RD (day/km)	1961–1990	−0.0297	−0.0119	−0.0049	−0.0068	−0.0062
	1991–2017	−0.0246	−0.0105	−0.0048	−0.0052	−0.0041
	Comparison	0.0051	0.0014	0.0001	0.0016	0.0021
RP (mm/day/km)	1961–1990	−0.0022	−0.0024	−0.0030	−0.0016	−0.0013
	1991–2017	−0.0025	−0.0025	−0.0036	−0.0020	−0.0015
	Comparison	−0.0003	−0.0001	−0.0006	−0.0004	−0.0002

4.2. Effect of Climate Change on Spatiotemporal Variations of Precipitation

The changes in the rain pattern are the direct result of the changes in RA, RD, and RP. Figures 10–12 illustrate the changes of different precipitation indices of different precipitation grades with distance from the sea. First, the significant increase of SRA led to an increase in annual RA (Figure 10a). LRD decreased significantly, which led to a decrease in RD, while the LRD and MRD increases led to increased RD at the XN, HLH, DBC, and BL stations (Figure 11a). LRP of annual rose slightly at all stations except QD. MRP of annual increased significantly at HLH, DBC, and BL stations, while SRP increased significantly at FZ, NC, and WH stations. There were also appeared HR and TR in arid areas in recent years (Figure 12a). Second, the decrease in LRA was roughly the same as the increase

in SRA, resulting in weak RA change in the spring (Figure 10b). The decreases of LRD and MRD caused the RD to decrease in the spring (Figure 11b). Spring RP of different levels of rainfall increased slightly in all regions (Figure 12b). Third, the increase of RA in summer was mainly reflected in the increase of SRA (Figure 10c), while the decrease of RD was mainly reflected in the decrease of LRD (Figure 11c). And the increase of LRP and SRP caused the summer RP increased (Figure 12c). Fourth, the significant decrease of the RA in autumn was mainly due to the significant decreases of LRA and MRA (Figure 10d), while the decrease of RD was also represented by the significant decreases of LRD and MRD (Figure 11d). The increase of autumn RP was caused by the increase of LRP (Figure 12d). Finally, the significant increase of RA in winter was mainly reflected in the increases of LRA, MRA, and HRA in the humid and semi-humid regions, while in the arid and semi-arid areas was caused by the significant increase of LRA (Figure 10e). The decrease of winter RD was caused by the decrease of MRD and HRD at FZ, NC, WH, and AK stations, while the significant increase of winter RD in the area after the 800 mm precipitation contour was caused by the significant increase of LRD (Figure 11e). The significant increase of winter RP was mainly caused by the significant increase of LRP (Figure 12e). Therefore, the SRA increased in summer and the LRA increased in winter, which explained the increases of RP in summer and winter. In addition, the decrease of LRD was the reason for the decrease of RD. It is obvious that the SRA increased significantly at FZ, NC, WH, and AK, while the LRD decreased significantly at these stations before 400 mm precipitation contour and increased significantly at these stations after 400 mm precipitation contour (Figures 10 and 11). Meanwhile, the RA and RD of different precipitation grades did not increase or decrease uniformly (Figure 12). Therefore, the increase of RP did not directly depend on the RP increases of different precipitation grades. Rather, it was caused by the significant decrease of LRD and the significant increase of SRA. Thus, the reason for the increase of precipitation in Northwest China was the increase of precipitation frequency, while the effect of increased precipitation intensity was more obvious in Southeast China [34].

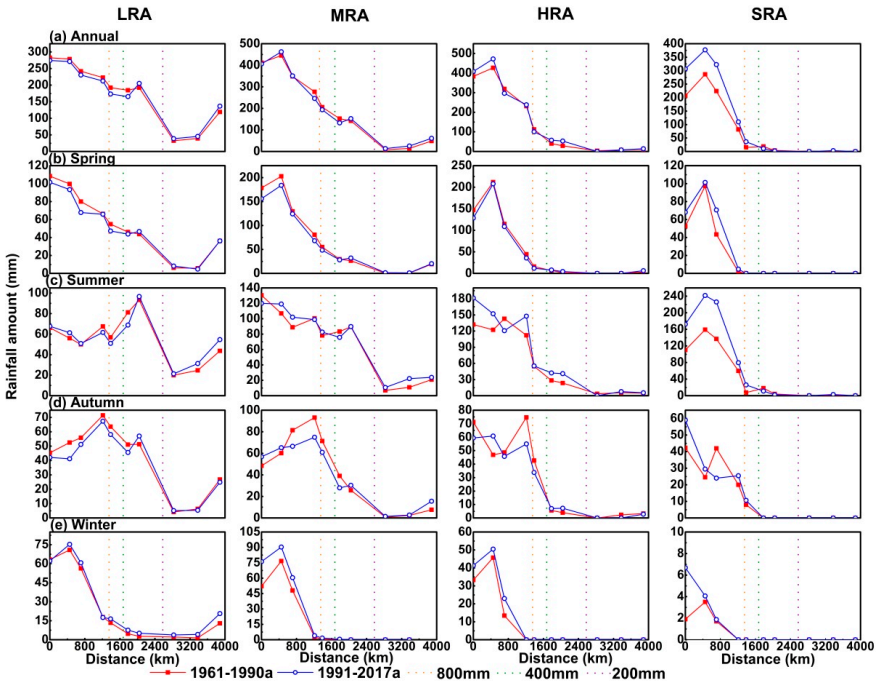

Figure 10. Changes of different grades of precipitation amount with distance from the sea, including light rainfall amount (LRA), moderate rainfall amount (MRA), heavy rainfall amount (HRA), and storm amount (SRA). Different grades of precipitation amount also include annual (**a**) and seasonal (including spring (**b**), summer (**c**), autumn (**d**) and winter (**e**)) variations. "800 mm" represents the 800-mm precipitation contour, "400 mm" represents the 400-mm precipitation contour, and "200 mm" represents the 200-mm precipitation contour.

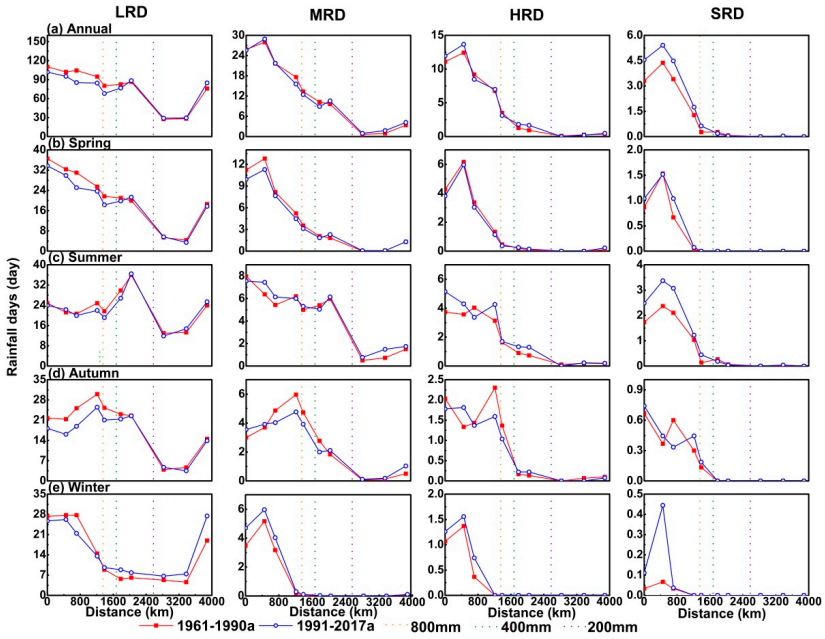

Figure 11. Changes of different grades of precipitation days with distance from the sea, including light rainfall days (LRD), moderate rainfall days (MRD), heavy rainfall days (HRD), and storm days (SRD). Different grades of precipitation amount also include annual (**a**) and seasonal (including spring (**b**), summer (**c**), autumn (**d**) and winter (**e**)) variations. "800 mm" represents the 800-mm precipitation contour, "400 mm" represents the 400-mm precipitation contour, and "200 mm" represents the 200-mm precipitation contour.

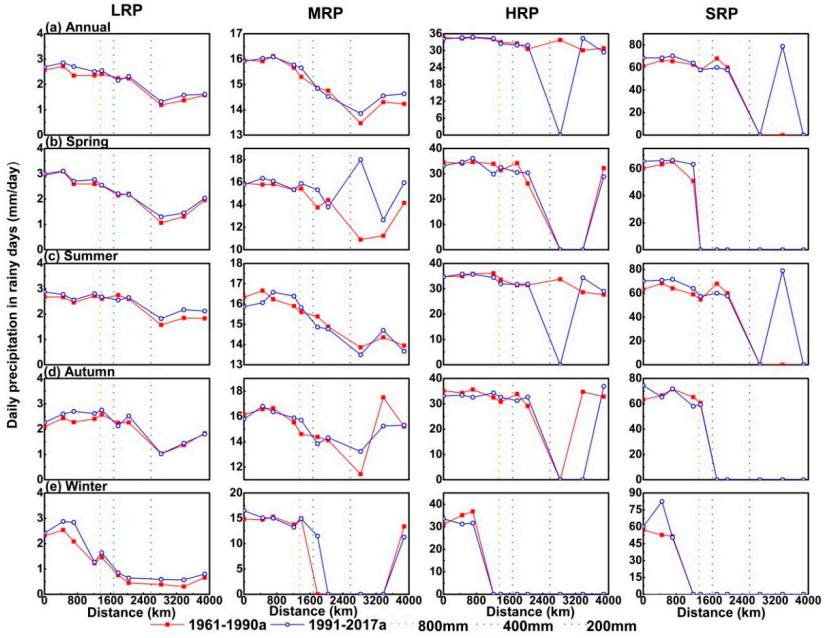

Figure 12. Changes of daily precipitation of different rainy day grades with distance from the sea, including daily precipitation on light rainfall days (LRP), daily precipitation on moderate rainfall days (MRP), daily precipitation on heavy rainfall days (HRP), and daily precipitation on stormy days (SRP). Different grades of precipitation amount also include annual (**a**) and seasonal (including spring (**b**), summer (**c**), autumn (**d**) and winter (**e**)) variations. "800 mm" represents the 800-mm precipitation contour, "400 mm" represents the 400-mm precipitation contour, and "200 mm" represents the 200-mm precipitation contour.

In addition, climate change is the driving force behind the changes in RA, RD, and RP. Global warming is one of the typical manifestations of climate change and has a direct impact on precipitation [4,64]. The annual average surface temperature in China increased significantly during the study period, and its warming range was slightly greater than the world average in the same time span [40]. It can be seen from Figure 13 that from 1961 to 2017, the average daily temperature in both year and seasons in the line from southeast to northwest of China increased, but there was no significant change in summer at AK and QD stations. The average daily temperature rise rates of the whole southeast to northwest line in annual, spring, summer, autumn, and winter were 0.24 °C/10 year, 0.26 °C/10 year, 0.16 °C/10 year, 0.23 °C/10 year, and 0.26 °C/10 year, respectively. Especially, the northwest arid region and the southeast humid region had a relatively large temperature increase. In terms of global average, the annual precipitation increases as the world warms [65]. Moreover, global warming also increases the frequency of extreme precipitation events [5,6]. Therefore, the rising temperatures may lead to higher RA and RP. Table 4 shows the correlation between annual and seasonal average daily temperature and precipitation indices of each station. It can be seen from the table that the correlation between temperature and precipitation at each station was not consistent, which was related to the nature of precipitation at each place. However, the annual RP of FZ, NC, and WH in the southeast had a strong positive correlation with the average daily temperature, and the annual and summer RD of FZ, NC, WH, AK, QD, YZ, and XN had a strong negative correlation with the average daily temperature. Therefore, the temperature may have more influence on the number of precipitation days. The rising temperature reduces the number of precipitation days, while the heavy precipitation increases.

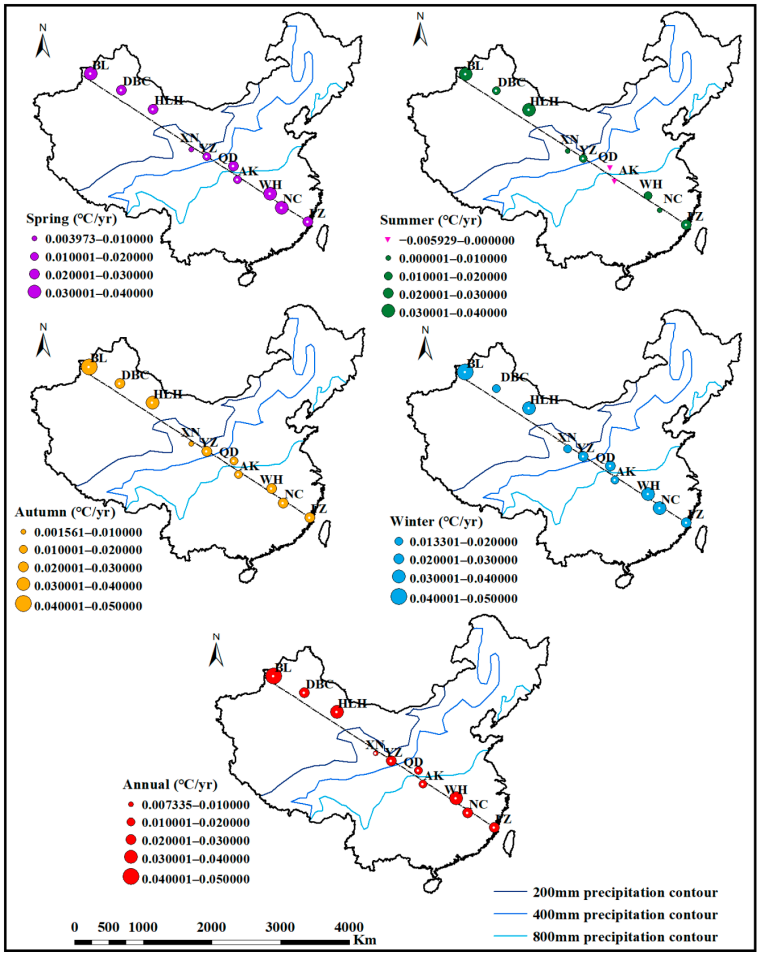

Figure 13. The Sen's slope of Mann-Kendall trend test was used to reflect the variation trends for the average daily temperature from 1961 to 2017. Note: white spots mean precipitation change trend reached the significance level of 95% confidence for the MK trend test.

Table 4. Pearson's correlation coefficients between precipitation indices and average daily temperature at each meteorological station during 1961–2017.

Stations	Indices	Spring	Summer	Autumn	Winter	Annual
FZ	RA	−0.48 *	−0.24	−0.02	0.12	0.19
	RD	−0.63 *	−0.44 *	−0.15	0.02	−0.22
	RP	−0.22	−0.10	−0.01	0.16	0.37 *
NC	RA	−0.42 *	−0.50 *	−0.15	−0.05	0.00
	RD	−0.59 *	−0.62 *	−0.35 *	−0.20	−0.39 *
	RP	−0.18	−0.18	0.14	0.06	0.27 *
WH	RA	−0.18	−0.32 *	−0.30 *	0.31 *	−0.01
	RD	−0.59 *	−0.58 *	−0.51 *	−0.11	−0.53 *
	RP	0.22	−0.03	0.01	0.36 *	0.31 *
AK	RA	−0.24	−0.57 *	−0.35 *	0.12	−0.40 *
	RD	−0.40 *	−0.67 *	−0.34 *	0.01	−0.56 *
	RP	0.04	−0.24	−0.29 *	0.17	−0.04
QD	RA	−0.34 *	−0.47 *	−0.25	−0.03	−0.26 *
	RD	−0.54 *	−0.66 *	−0.33 *	−0.15	−0.48 *
	RP	0.03	−0.12	−0.14	0.16	0.07
YZ	RA	−0.08	−0.47 *	−0.24	0.05	−0.32 *
	RD	−0.31 *	−0.53 *	−0.16	−0.02	−0.42 *
	RP	0.18	−0.29 *	−0.15	0.27 *	−0.09
XN	RA	0.15	−0.23	−0.09	0.00	−0.14
	RD	−0.02	−0.44 *	−0.25	−0.12	−0.25
	RP	0.23	−0.02	0.12	0.08	0.01
HLH	RA	−0.08	−0.25	0.15	−0.19	0.02
	RD	−0.17	−0.47 *	0.10	−0.32 *	−0.03
	RP	−0.05	−0.03	0.13	0.17	0.04
DBC	RA	−0.13	−0.05	0.07	0.02	0.05
	RD	−0.25	−0.14	−0.22	0.00	0.00
	RP	0.09	−0.03	0.11	0.15	0.07
BL	RA	−0.12	0.02	0.18	0.19	0.24
	RD	−0.28 *	−0.03	−0.07	0.08	0.22
	RP	0.06	0.04	0.25	0.19	0.15

Note: * significant at 0.05 level.

Last, one of the characteristics of China's climate is the significant monsoon pattern [66]. Further analysis shows that the precipitation in China is primarily affected by the monsoon, with the exception of the northwestern region. The summer precipitation in southeastern China is mainly impacted by both the Indian monsoon and the East Asian summer monsoon. In addition, the positive (or negative) temperature anomalies over Europe and the Atlantic Ocean regions are favorable to more (or less) water vapor content over southeastern China [67]. The strength of the East Asian summer monsoon and its associated rainfall are related to the western North Pacific subtropical high on the East Asian continent [39,67,68]. The zonal migration of the western North Pacific subtropical high will lead to abnormal climate conditions in China [69]. Therefore, the increase of extreme precipitation in the summer may be due to changes in the Indian monsoon, East Asian summer monsoon, and western North Pacific subtropical high. The degree of change in summer precipitation reflects the degree to which these climate factors have changed. Therefore, the intensity of the summer monsoon may have increased. The precipitation in winter is mainly influenced by the East Asian winter monsoon. Due to the interaction between the Siberian high and the Aleutian low, northwest winds prevail. The East Asian winter monsoon causes most parts of China to be cold and dry in winter, although rain and snow can form when cold, dry air at high latitudes meets warm, moist air from low latitudes [70]. The decrease or increase in surface temperatures over East Asia is significantly correlated with the

strength or weakness of the East Asian winter monsoon [71]. In recent years, however, the surface temperatures in China have increased significantly and the precipitation in winter has also increased significantly. It can thus be inferred that the East Asian winter monsoon is weakening. This is also consistent with the general theory that China's overall winter precipitation is lower in harsh winters and higher in mild winters [72]. In Northwest China, the main reason for the significantly increasing trend of precipitation may be the strengthening of the western North Pacific subtropical high and the North American subtropical high [35].

4.3. Effects of Terrain on Precipitation Change

The complex and varied terrain also has a significant impact on precipitation in China. Dirmeyer [73] (1998) found that the geography of land and sea influences the monsoon circulation. When compared with the topographic map of China, it is clear the spatial variation of precipitation in China is also affected by the topography, especially the variations in elevation [74]. As the distance from the sea increases, the intensity of the monsoon effect decreases. The "three staircases" of China are situated such that the terrain is high in the west and low in the east. Therefore, the high mountain ranges act as a barrier, making it difficult for water vapor from the sea to flow to the northwest. In this study, in general, RA, RD and RP were also found to decrease with increasing distance from the sea. Not all of the precipitation indices decreased directly with increasing sea distance, however. The annual RA and RP increased from the FZ to NC stations and decreased sharply at QD (Figure 7). The monsoon influence at FZ was less at NC due to the impact of the Taiwan Mountains. Since the heights of the Taiwan Mountains vary from 3 to 3.5 km and FZ is approximately 250 km from this mountain range, the blocking effect of the mountains is strong. Due to the blocking effect of the mountains in Taiwan, the monsoon exerted little effect on the precipitation at FZ, resulting in less precipitation at FZ than at NC. In addition, the transition from WH to QD is essentially from the humid region to the sub-humid region, which leads to a change in the climate conditions, including a change in the precipitation. QD is located to the north of the Qinling Mountains. The mountains block moisture from the ocean, causing a sharp drop in rainfall. In addition to these abnormal points, precipitation from HLH to BL showed an upward trend with the increase of distance from the sea. Combined with Table 1 and Figure 1, it is found that the altitude of HLH, DBC, and BL decreases in turn. As the northwest is far away from the sea, the influence of the monsoon is weakened, and the landform is the main factor affecting the rainfall. And the monsoon's degree of influence on precipitation varies with distance from the sea. The influence degree of the monsoon reached its maximum at the WH station in the middle and lower reaches of the Yangtze River, and reached its minimum at the YZ station in the semi-arid region (Figure 9). The monsoon also exerted a large impact on RD. A significant decrease in RD led to an increase of heavy or strong precipitation in southeast and central China. In Northwest China beyond YZ, RP increased due to the increase in the RD of light precipitation.

5. Conclusions

The purposes of this study were to investigate the spatiotemporal precipitation changes from southeast to northwest China and to explore the factors that influence these changes. The following conclusions were drawn:

(1) From 1961 to 2013, the temporal changes of precipitation exhibited increasing trends, and precipitation changes mainly occurred in summer and winter. The annual precipitation change was similar to the changes in summer and winter: the RA and RP generally increased. The RD in arid and semi-arid areas increased noticeably, and decreased obviously in humid and semi-humid regions. The RD decreased significantly in spring, and the autumn RA and RD decreased in most areas.

(2) On the whole, RA, RD, and RP decreased with the increase of distance from the sea; the RA and RP increased from the FZ to NC stations and decreased sharply at QD. The precipitation indices showed an upward trend from HLH to BL. Compared with the standard climate period of

1961–1990, the precipitation changed significantly from 1991 to 2017: the obvious RD reductions caused annual, spring, and winter RP increases; the RA increase led to the RP increase in summer; the RD reduction that was greater than the RA decrease led to the increased RP in autumn. The spatial variation of the change trends of the precipitation indices also displayed some regularity. The heavy or strong precipitation increased in southeastern and central China, while the weak precipitation increased in northwestern China.

(3) Climate change affected the precipitation change. First, the higher temperatures led to increased precipitation. Second, the strengthening of the summer monsoon caused summer extreme precipitation to increase, while the weakening of the winter monsoon led to an increase in wintertime light precipitation. Third, the change of climate or monsoon altered the rates of precipitation decrease with distance from the sea: RA and RP decreased faster, compared with 1961–1990, the annual decline rate of RA and RP increased to 6% and 13.6%, respectively; RD decrease slower, the rates of the annual, summer, and winter RA decreases were faster, while the spring and autumn rates were slower, and compared with 1961–1990, the annual decline rate of RD decreased to 17.2%. Finally, terrain also exhibits a pronounced impact on precipitation in China.

This study did not examine the responses of precipitation changes and other climate factors changes. In the future, we plan to analyze the responses of precipitation, characterize the major factors of climate change and predictive climate model. The results of the current investigation revealed that precipitation is affected by climate change and that precipitation change can reflect climate change. The total precipitation and precipitation intensity from southeast to northwest China have increased significantly, which poses a challenge to the rational utilization of water resources in China. From the southeast to the northwest, different regions should adopt different measures and management modes in order to optimize the use of water resources.

Author Contributions: Data curation, Z.L.; Formal analysis, H.L.; Writing—original draft, Z.L.; Writing—review & editing, H.L. All authors have read and agreed to the published version of the manuscript.

Funding: This research was supported by the National Key R&D Program of China (No. 2017YFE0118100-2), the One Hundred Person Project of Shannxi Province ([2017]35), Key Research and Development program of Shaanxi Province (No. 2020NY-174), and Central Public-interest Scientific Institution Basal Research Fund of China (No. CKSF2019292/SH+TB).

Acknowledgments: We thank Wenting Wang for providing some suitable revisions for this manuscript. The authors gratefully acknowledge the meteorological data received from the National Meteorological Center of the China Meteorological Administration (https://cmdp.ncc-cma.net/cn).

Conflicts of Interest: The authors declare no conflict of interest.

References

1. Allen, M.R.; Ingram, W.J. Constraints on future changes in climate and the hydrologic cycle. *Nature* **2002**, *419*, 224–232. [CrossRef] [PubMed]
2. Stocker, T.F.; Raible, C.C. Water cycle shifts gear. *Nature* **2005**, *434*, 830–833. [CrossRef] [PubMed]
3. Ziegler, A.D.; Sheffield, J.; Maurer, E.P.; Nijssen, B.; Wood, E.F.; Lettenmaier, D.P. Detection of intensification in global- and continental-scale hydrological cycles: Temporal scale of evaluation. *J. Clim.* **2003**, *16*, 535–547. [CrossRef]
4. Zhang, Q.; Li, J.; Singh, V.P.; Xiao, M. Spatio-temporal relations between temperature and precipitation regimes: Implications for temperature-induced changes in the hydrological cycle. *Glob. Planet. Chang.* **2013**, *111*, 57–76. [CrossRef]
5. Kunkel, K.E. North American trends in extreme precipitation. *Nat. Hazards* **2003**, *29*, 291–305. [CrossRef]
6. IPCC. Summary for Policy makers. In *Climate Change 2013: The Physical Science Basis. Contribution of Working Group I to the Fifth Assessment Report of the Intergovernmental Panel on Climate Change*; Cambridge University Press: Cambridge, UK; New York, NY, USA, 2013.

7. Mirza, M.M.Q. Global warming and changes in the probability of occurrence of floods in Bangladesh and implications. *Glob. Environ. Chang.* **2002**, *12*, 127–138. [CrossRef]
8. Schmidhuber, J.; Tubiello, N.F. Global food security under climate change. *Proc. Natl. Acad. Sci. USA* **2007**, *104*, 19703–19708. [CrossRef]
9. Min, S.K.; Zhang, X.; Zwiers, F.W.; Hegerl, G.C. Human contribution to more-intense precipitation extremes. *Nature* **2011**, *470*, 378–381. [CrossRef]
10. Liu, L.; Xu, Z.X. Regionalization of precipitation and the spatiotemporal distribution of extreme precipitation in Southwestern China. *Nat. Hazards* **2016**, *80*, 1195–1211. [CrossRef]
11. Allan, R.P.; Soden, B.J. Atmospheric Warming and the Amplification of Precipitation Extremes. *Science* **2008**, *321*, 1481–1484. [CrossRef]
12. Giorgi, F.; Raffaele, F.; Coppola, E. The response of precipitation characteristics to global warming from climate projections. *Earth Syst. Dynam.* **2019**, *10*, 73–89. [CrossRef]
13. Myhre, G.; Alterskjær, K.; Stjern, C.W.; Hodnebrog, Ø.; Marelle, L.; Samset, B.H.; Sillmann, J.; Schaller, N.; Fischer, E.; Schulz, M.; et al. Frequency of extreme precipitation increases extensively with event rareness under global warming. *Sci. Rep.* **2019**. [CrossRef] [PubMed]
14. Zhang, X.; Vincent, L.A.; Hogg, W.D.; Niitsoo, A. Temperature and precipitation trends in Canada during the 20th century. *Atmos. Ocean.* **2000**, *38*, 395–429. [CrossRef]
15. Mekis, É.; Vincent, L.A. An overview of the second generation adjusted daily precipitation dataset for trend analysis in Canada. *Atmos. Ocean.* **2011**, *49*, 163–177. [CrossRef]
16. Vincent, L.A.; Zhang, X.; Mekis, E.; Wan, H.; Bush, E.J. Changes in Canada's climate: Trends in indices based on daily temperature and precipitation data. *Atmos. Ocean.* **2018**, *56*, 332–349. [CrossRef]
17. Karl, T.R.; Knight, R.W. Secular trends of precipitation amount, frequency, and intensity in the United States. *Bull. Am. Meteorol. Soc.* **1998**, *79*, 231–241. [CrossRef]
18. Raghavendra, A.; Dai, A.; Milrad, S.M.; Cloutier-Bisbee, S.R. Floridian heatwaves and extreme precipitation: Future climate projections. *Clim. Dynam.* **2018**, *52*, 495–508. [CrossRef]
19. Swain, D.L.; Langenbrunner, B.; Neelin, J.D.; Hall, A. Increasing precipitation volatility in twenty-first-century California. *Nat. Clim. Chang.* **2018**, *8*, 427–433. [CrossRef]
20. Wang, H.; Fu, R. Cross-equatorial flow and seasonal cycle of precipitation over South America. *J. Clim.* **2002**, *15*, 1591–1608. [CrossRef]
21. Liebmann, B.; Vera, C.S.; Carvalho, L.M.V.; Camilloni, I.A.; Hoerling, M.P.; Allured, D.; Barroset, V.; Báez, J.; Bidegain, M. An observed trend in central South American precipitation. *J. Clim.* **2004**, *17*, 4357–4367. [CrossRef]
22. Zolina, O.; Simmer, C.; Gulev, S.K.; Kollet, S. Changing structure of European precipitation: Longer wet periods leasing to more abundant rainfalls. *Geophys. Res. Lett.* **2010**, *37*, 460–472. [CrossRef]
23. Madsen, H.; Lawrence, D.; Lang, M.; Martinkova, M.; Kjeldsen, T.R. Review of trend analysis and climate change projections of extreme precipitation and floods in Europe. *J. Hydrol.* **2014**, *519*, 3634–3650. [CrossRef]
24. Kruger, A.C. Observed trends in daily precipitation indices in South Africa: 1910–2004. *Int. J. Climatol.* **2006**, *26*, 2275–2285. [CrossRef]
25. Shongwe, M.; Van Oldenborgh, G.J.; Hurk, B.; De Boer, B.; Coelho, S.; Aalst, M. Projected changes in mean and extreme precipitation in Africa under global warming. part i: Southern Africa. *J. Clim.* **2009**, *22*, 3819–3837. [CrossRef]
26. Roy, S.S.; Balling, R.C., Jr. Trends in extreme daily precipitation indices in India. *Int. J. Climatol.* **2004**, *24*, 457–466.
27. Endo, N.; Matsumoto, J.; Lwin, T. Trends in precipitation extremes over Southeast Asia. *Sola* **2009**, *5*, 168–171. [CrossRef]
28. Limsakul, A.; Singhruck, P. Long-term trends and variability of total and extreme precipitation in Thailand. *Atmos. Res.* **2016**, *169*, 301–317. [CrossRef]
29. Yang, T.; Li, Q.; Chen, X.; Maeyer, P.D.; Yan, X.; Liu, Y.; Zhao, T.; Li, L. Spatiotemporal variability of the precipitation concentration and diversity in Central Asia. *Atmos. Res.* **2019**. [CrossRef]
30. Partal, T.; Kahya, E. Trend analysis in Turkish precipitation data. *Hydrol. Process.* **2006**, *20*, 2011–2026. [CrossRef]
31. Rahimzadeh, F.; Asgari, A.; Fattahi, E. Variability of extreme temperature and precipitation in Iran during recent decades. *Int. J. Climatol.* **2009**, *29*, 329–343. [CrossRef]

32. Tabari, H.; Talaee, P.H. Temporal variability of precipitation over Iran: 1966–2005. *J. Hydrol.* **2011**, *396*, 313–320. [CrossRef]
33. Sun, Y.; Ding, Y.H. A projection of future changes in summer precipitation and monsoon in East Asia. *Sci. China Earth Sci.* **2010**, *53*, 284–300. (In Chinese) [CrossRef]
34. Zhai, P.M.; Zhang, X.B.; Wan, H.; Pan, X.H. Trends in Total Precipitation and Frequency of Daily Precipitation Extremes over China. *J. Clim.* **2005**, *18*, 1096–1108. [CrossRef]
35. Li, B.; Chen, Y.; Chen, Z.; Xiong, H.; Lian, L. Why does precipitation in northwest China show a significant increasing trend from 1960 to 2010? *Atmos. Res.* **2016**, *167*, 275–284. [CrossRef]
36. Yang, P.; Xia, J.; Zhang, Y.; Hong, S. Temporal and spatial variations of precipitation in Northwest China during 1960–2013. *Atmos. Res.* **2017**, *183*, 283–295. [CrossRef]
37. Tan, L.; Cai, Y.; An, Z.; Cheng, H.; Shen, C.C.; Gao, Y.; Edwards, R.L. Decreasing monsoon precipitation in Southwest China during the last 240 years associated with the warming of Tropical Ocean. *Clim. Dynam.* **2016**, *48*, 1769–1778. [CrossRef]
38. Gu, W.; Wang, L.; Hu, Z.Z.; Hu, K.; Li, Y. Interannual Variations of the First Rainy Season Precipitation over South China. *J. Clim.* **2018**, *31*, 623–640. [CrossRef]
39. Zhang, Q.; Zheng, Y.; Singh, V.P.; Luo, M.; Xie, Z. Summer extreme precipitation in Eastern China: Mechanisms and impacts. *J. Geophys. Res. Atmos.* **2017**, *122*, 2766–2778. [CrossRef]
40. Ding, Y.; Ren, G.; Zhao, Z.; Xu, Y.; Luo, Y.; Li, Q.; Zhang, J. Detection, causes and projection of climate change over China: An over view of recent progress. *Adv. Atmos. Sci.* **2007**, *24*, 954–971. [CrossRef]
41. Gong, D.Y.; Shi, P.J.; Wang, J.A. Daily precipitation changes in the semi-arid region over northern china. *J. Arid. Environ.* **2004**, *59*, 771–784. [CrossRef]
42. Zhang, Q.; Peng, J.T.; Singh, V.P.; Li, J.F.; Chen, Y.D. Spatio-temporal variations of precipitation in arid and semiarid regions of China: The Yellow River basin as a case study. *Glob. Planet. Chang.* **2014**, *114*, 38–49. [CrossRef]
43. Mosmann, V.; Castro, A.; Fraile, R.; Dessens, J.; Sánchez, J.L. Detection of statistically significant trends in the summer precipitation of mainland Spain. *Atmos. Res.* **2004**, *70*, 43–53. [CrossRef]
44. Mann, H.B. Nonparametric tests against trend. *Econometrica* **1945**, *13*, 245–259. [CrossRef]
45. Kendall, M.G. *Rank Correlation Methods*; Griffin: London, UK, 1955.
46. Mitchell, J.M.; Dzerdzeevskii, B.; Flohn, H.; Hofmeyr, W.L.; Lamb, H.H.; Rao, K.N.; Wallén, C.C. *Climate Change*; WMO Technical Note No.79; World Meteorological Organization: Geneva, Switzerland, 1966; p. 79.
47. von Storch, H. Misuses of Statistical Analysis in Climate Research. In *Analysis of Climate Variability: Applications of Statistical Techniques*; Springer: New York, NY, USA, 1995; pp. 11–26. [CrossRef]
48. Douglas, E.M.; Vogel, R.M.; Kroll, C.N. Trends in floods and low flows in the United States: Impact of spatial correlation. *J. Hydrol.* **2000**, *240*, 90–105. [CrossRef]
49. Zhang, X.; Harvey, K.D.; Hogg, W.D.; Yuzyk, T.R. Trends in Canadian streamflow. *Water. Resour. Res.* **2001**, *37*, 987–998. [CrossRef]
50. Bayazit, M.; Önöz, B. To prewhiten or not to prewhiten in trend analysis? *Hydrolog. Sci. J.* **2007**, *52*, 611–624. [CrossRef]
51. Theil, H. A rank-invariant method of linear and polynomial regression analysis, III. *Proc. Ned. Akad. Wet.* **1950**, *53*, 1397–1412.
52. Sen, P.K. Estimates of the Regression Coefficient Based on Kendall's Tau. *J. Am. Stat. Assoc.* **1968**, *63*, 1379–1389. [CrossRef]
53. Wang, R.; Zhang, J.Q.; Guo, E.L.; Zhao, C.L.; Cao, T.H. Spatial and temporal variations of precipitation concentration and their relationships with large-scale atmospheric circulations across Northeast China. *Atmos. Res.* **2019**, *222*, 62–73. [CrossRef]
54. Zhao, Z.C.; Luo, Y.; Wang, S.W.; Huang, J.B. Science issues on global warming. *J. Meteorol. Environ.* **2015**, *31*, 1–5. (In Chinese)
55. Liu, B.; Xu, M.; Henderson, M.; Qi, Y. Observed trends of precipitation amount, frequency, and intensity in China, 1960–2000. *J. Geophys. Res. Atmos.* **2005**. [CrossRef]
56. Zhang, Q.; Xu, C.Y.; Zhang, Z.; Chen, Y.D.; Liu, C.L. Spatial and temporal variability of precipitation over China, 1951–2005. *Theor. Appl. Climatol.* **2009**, *95*, 53–68. [CrossRef]
57. Su, Y.; Zhao, C.; Wang, Y.; Ma, Z. Spatiotemporal Variations of Precipitation in China Using Surface Gauge Observations from 1961 to 2016. *Atmosphere* **2020**, *11*, 303. [CrossRef]

58. Zhang, Q.; Singh, V.P.; Sun, P.; Chen, X.; Zhang, Z.; Li, J. Precipitation and streamflow changes in China: Changing patterns, causes and implications. *J. Hydrol.* **2011**, *410*, 204–216. [CrossRef]
59. Feng, Y.; Zhao, X. Changes in spatiotemporal pattern of precipitation over China during 1980–2012. *Environ. Earth. Sci.* **2015**, *73*, 1649–1662. [CrossRef]
60. Li, J.; Yu, R.; Yuan, W.; Chen, H. Changes in duration-related characteristics of late-summer precipitation over eastern China in the past 40 years. *J. Clim.* **2011**, *24*, 5683–5690. [CrossRef]
61. Tao, S.Y.; Chen, L.X. A review of recent research of the East Asian summer monsoon in China. In *Monsoon Meteorology*; Chang, C.P., Krishnamurti, T.N., Eds.; Oxford University Press: New York, NY, USA, 1987; pp. 60–92.
62. Gao, Z.H. Analysis of the characteristics of China precipitation changes during 1961–2011. *Clim. Chang. Res. Lett.* **2013**, *2*, 147–152. (In Chinese)
63. Zhang, Q.; Xu, C.Y.; Chen, X.; Zhang, Z. Statistical behaviours of precipitation regimes in China and their links with atmospheric circulation 1960–2005. *Int. J. Climatol.* **2011**, *31*, 1665–1678. [CrossRef]
64. Trenberth, K.E. Changes in precipitation with climate change. *Clim. Res.* **2011**, *47*, 123–138. [CrossRef]
65. Chou, C.; Lan, C. Changes in the annual range of precipitation under global warming. *J. Clim.* **2012**, *25*, 222–235. [CrossRef]
66. Qin, D.; Tao, S.; Dong, S.; Luo, Y. Climate, Environmental, and Socioeconomic Characteristics of China. In *Climate and Environmental Change in China: 1951–2012*; Qin, D., Ding, Y., Mu, M., Eds.; Springer: Berlin/Heidelberg, Germany, 2016.
67. Wang, H.; Chen, H. Climate control for southeastern China moisture and precipitation: Indian or East Asian monsoon? *J. Geophys. Res.* **2012**. [CrossRef]
68. Lin, Z.; Wang, B. Northern East Asian low and its impact on the interannual variation of East Asian summer rainfall. *Clim. Dynam.* **2016**, *46*, 83–97. [CrossRef]
69. Lu, R.; Li, Y.; Ryu, C.S. Relationship between the zonal displacement of the western Pacific subtropical high and the dominant modes of low-tropospheric circulation in summer. *Prog. Nat. Sci.* **2008**, *18*, 161–165.
70. Wang, S.W.; Wen, X.Y.; Huang, J.B. East Asian winter monsoon. *Clim. Chang. Res.* **2013**, *9*, 154–156. (In Chinese) [CrossRef]
71. Ha, K.-I.; Heo, K.Y.; Lee, S.S.; Yun, K.S.; Jhun, J.G. Variability in the East Asian Monsoon: A review. *Meteorol. Appl.* **2012**, *19*, 200–215. [CrossRef]
72. Wang, L.; Chen, W. How well do existing indices measure the strength of the East Asian winter monsoon? *Adv. Atmos. Sci.* **2010**, *27*, 855–870. [CrossRef]
73. Dirmeyer, P.A. Land-sea geometry and its effect on monsoon circulations. *J. Geophys. Res.* **1998**, *103*, 11555–11572. [CrossRef]
74. Fu, B. The influence of topography and altitude on precipitation. *Acta Geogr. Sin.* **1992**, *4*, 302–314. (In Chinese)